HOKKAIDO UNIVERSITY

Title	Sub-Terahertz MIMO Spatial Multiplexing in Indoor Propagation Environments
Author(s)	Ogawa, Yasutaka; Utsuno, Taichi; Nishimura, Toshihiko; Ohgane, Takeo; Sato, Takanori
Citation	IEICE transactions on communications, E105B(10), 1130-1138 https://doi.org/10.1587/transcom.2021MEI0004
Issue Date	2022-10-01
Doc URL	http://hdl.handle.net/2115/87544
Type	article
File Information	E105.B_2021MEI0004.pdf

Instructions for use

INVITED PAPER   *Special Section on Multidisciplinary and Innovative Key technologies in Advanced communication systems (MIKA)*

Sub-Terahertz MIMO Spatial Multiplexing in Indoor Propagation Environments

Yasutaka OGAWA[†a)], *Fellow*, Taichi UTSUNO[†], *Student Member*, Toshihiko NISHIMURA[†], *Senior Member*, Takeo OHGANE[†], *Fellow*, and Takanori SATO[†], *Member*

SUMMARY   A sub-Terahertz band is envisioned to play a great role in 6G to achieve extreme high data-rate communication. In addition to very wide band transmission, we need spatial multiplexing using a hybrid MIMO system. A recently presented paper, however, reveals that the number of observed multipath components in a sub-Terahertz band is very few in indoor environments. A channel with few multipath components is called sparse. The number of layers (streams), i.e. multiplexing gain in a MIMO system does not exceed the number of multipaths. The sparsity may restrict the spatial multiplexing gain of sub-Terahertz systems, and the poor multiplexing gain may limit the data rate of communication systems. This paper describes fundamental considerations on sub-Terahertz MIMO spatial multiplexing in indoor environments. We examined how we should steer analog beams to multipath components to achieve higher channel capacity. Furthermore, for different beam allocation schemes, we investigated eigenvalue distributions of a channel Gram matrix, power allocation to each layer, and correlations between analog beams. Through simulation results, we have revealed that the analog beams should be steered to all the multipath components to lower correlations and to achieve higher channel capacity.

key words: *6G, sub-Terahertz band, hybrid MIMO system, spatial multiplexing, channel capacity, beam steering*

1. Introduction

Now that fifth generation (5G) services in mobile communication have been commercially available, sixth generation (6G) techniques are being extensively studied in industry and academia [1]–[6]. One of the requirements in 6G is extreme high data-rate communication over 100 Gbps, which is much above that in 5G, about 10 Gbps. To realize such high-speed communication, we need to use a Terahertz band above 100 GHz where an extremely wide bandwidth is available. Many studies have been done on this field [7]–[10]. A frequency range of 100–300 GHz will be used in 6G, and the spectrum is called a sub-Terahertz band [10].

The most critical issue in using such a high frequency range is large propagation loss. Thus, we need high-gain directional antennas, which are realized using arrays with a large number of antenna elements, often called ultra-massive MIMO systems [11]. To realize such systems, a fully-digital beamforming architecture is one selection. In the architecture, however, each antenna owns a dedicated RF chain and digital-analog-converter/analog-digital-converter, which consume much power. The hardware complexity and power consumption of the fully-digital beamforming architecture are unbearable for practical use [12]. Thus, a hybrid beamforming architecture has been treated as a realistic technology [12], [13]. The architecture consists of a low-dimensional digital beamformer and an RF analog beamformer with phase shifters [14].

In addition to wideband transmission, we need spatial multiplexing to achieve extreme high data-rate communication. Reference [15] states that transmission over 100 Gbps is possible at a 100 GHz band using a MIMO system with a hybrid beamformer. The paper assumes a 16-path Nakagami-Rice fading channel with a Rician factor of 10 dB, which is the same channel condition for a millimeter wave band around 20 GHz stated in [16]. The critical issue is whether sub-Terahertz bands are such multipath-rich environments. Channel properties have been obtained for a 140 GHz band from measurement campaigns in indoor environments, and compared with those for a 28 GHz band [17], [18]. According to [18], the measurements were conducted for different TX-RX location pairs in a typical indoor office environment. The TX-RX distance ranged from 3.9 m to 45.9 m for 28 GHz and from 3.9 m to 39.2 m for 140 GHz. We consider that the measured results stated below show very important propagation characteristics in indoor environments.

The total number of observed subpaths (multipaths) at 140 GHz is much fewer than the number at 28 GHz. When the number of significant multipath components is low in a channel, the channel is called sparse [19]. Thus, the 140 GHz channel is much sparser than the channel at 28 GHz. The number of layers (streams) in a MIMO system does not exceed the number of multipaths. The sparsity may restrict the spatial multiplexing gain of sub-Terahertz systems, and the poor multiplexing gain may limit the data rate of systems. Note that multiplexing gain basically represents the ratio of data rates transmitted by a MIMO system to those by a single-input single-output (SISO) one, and several definitions have been presented [20]–[22]. In this paper, we define multiplexing gain as the number of available layers (streams).

Han et al. [12] proposed a widely-spaced multi-subarray hybrid beamforming architecture which realizes line-of-sight (LOS) MIMO communication by increasing the subarray interval. Although the architecture achieves

---

multiplexing in sparse environments, the array size is very big and unbearable for practical use.

This paper describes fundamental considerations on sub-Terahertz MIMO spatial multiplexing in indoor environments where the propagation characteristics follow the results in [18]. We assume that a base station (BS) has a hybrid beamforming architecture, which consists of several analog subarrays and a digital precoder. Each subarray works as a phased array and steers its beam in one of the multipath component directions. The digital precoder realizes optimum transmission using singular value decomposition of a channel matrix and water-filling [27]. We assume that the number of multipaths is fewer than that of subarrays, and examine how we should allocate the beams of the subarrays to multipath components. Based on the sub-Terahertz channel model introduced in [18], we evaluate dependence of channel capacity on beam allocation. Furthermore, we investigate eigenvalue distributions of the channels, power allocation to each layer, and correlations between beams.

The rest of the paper is organized as follows. We review in brief MIMO-related techniques in Sect. 2. In Sect. 3, we explain the hybrid MIMO architecture and preliminaries to its performance evaluation. We briefly describe measured channel properties in a sub-Terahertz band in Sect. 4. In Sect. 5, we discuss the evaluation of the MIMO system using simulations. Finally, we conclude the paper in Sect. 6.

2. Review of MIMO-Related Techniques

Before we consider MIMO spatial multiplexing in a sub-Terahertz band, we briefly review MIMO-related techniques. We think that MIMO systems have developed from adaptive antennas [23], which can suppress interference in a spatial domain. One of the most important features of the adaptive antennas is to control its radiation pattern depending on environments. Forming nulls in the directions of interferences, the adaptive antennas cancel them. An important application of the adaptive antennas is space division multiple access (SDMA) in mobile communications [24]. A BS equipped with an adaptive antenna can accommodate multiple users on the same frequency and time slot [25]. The adaptive antennas, however, do not treat multiple stream transmission in a set of TX and RX.

In 1987, J. H. Winters evaluated data rate of communication systems with multiple antennas at both TX and RX sides in a Rayleigh fading environment [26]. In such multipath-rich environments, it is possible to realize spatial multiplexing in a set of TX and RX because all the channels are almost independent. To the best of our knowledge, the reference is the first presentation of a MIMO system, although the term of MIMO is not used in [26]. Moreover, E. Telatar proved that channel capacity is given by the total capacity of M_{min} SISO channels, where M_{min} is the minimum number of TX and RX antennas [27]. He also showed that channel capacity increases in proportion to the number of antennas when the number of TX antennas is the same as that of RX antennas. This discovery is very important for realizing high-speed wireless transmission. We can say that he established the MIMO information theory.

It is seen that channel capacity is limited by the minimum number of TX and RX antennas. In mobile communications, a BS has much more antennas than each UE, and the data rate with the MIMO system is limited by the number of UE antennas. If the BS simultaneously communicates with multiple UEs, the total number of UE antennas is larger and the sum data rate increases. This is a multi-user MIMO system, which is quite similar to SDMA. A multi-user MIMO system can realize multiple stream transmission between the BS and each UE. Thus, a multi-user MIMO system can be seen as a developed technique of SDMA. For downlink transmission, system performance suffers from multi-user interference. To reduce the interference, some techniques have been proposed such as block diagonalization [28].

Massive MIMO systems which have a large number of antennas at a BS have developed from small-scale MIMO technology [29]. They provide high beamforming gain and high spatial resolution. Massive MIMO technology was originally conceived for conventional sub-6 GHz frequencies, and can be realized by fully-digital beamforming architectures. It is also important for millimeter wave and sub-Terahertz bands. Massive MIMO systems at the higher frequency bands are quite different from those at sub-6 GHz because propagation behavior and hardware characteristics are different. As stated previously, they are implemented with hybrid beamforming architectures.

When installing a massive MIMO system, we can geographically deploy BS antennas over a cell. This is called distributed massive MIMO system which has several advantages such as enhanced coverage areas [30].

This is a description form adaptive antennas to distributed massive MIMO systems over five decades. We will state MIMO spatial multiplexing in a sub-Terahertz band from the next section.

3. Spatial Multiplexing with Hybrid MIMO Architecture

This paper treats downlink transmission. Figure 1 shows the MIMO system that we consider in this paper. The BS has N linear subarrays, and each subarray has isotropic N_s antenna elements with half-wavelength spacing. A phase shifter is connected to each antenna element, and each subarray works as a phased array. The spacing between adjacent subarrays is a half wavelength. The subarrays are connected to a precoder where digital processing is done. User equipment (UE) has an M-element linear array with half-wavelength spacing, and the antenna elements are isotropic. The array is followed by a postcoder.

Here, we consider the above antenna-related parameters and assumptions for the BS.

(1) In this paper, we assume that angles of departure (AODs) of all the multipath components have been available at the BS. In actual applications, we need to
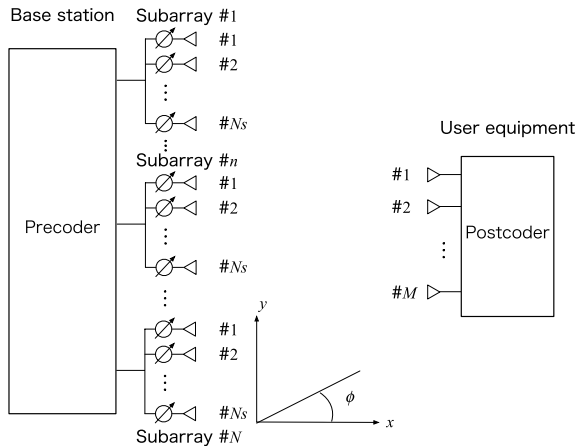
Fig. 1 MIMO system with hybrid beamforming architecture.

estimate them as will be stated in Sect. 3.1. The assumption of half-wavelength spacing of antennas in each subarray is reasonable because the subarrays are used also for the AOD estimation. The spacing larger than a half wavelength generates grating lobes, and the smaller spacing causes lower resolution.

(2) If the spacing between adjacent subarrays is larger than a half wavelength, the performance will be better because correlations between multipath components are lower. It is, however, unlikely that the spacing changes basic MIMO spatial multiplexing performance drastically unless it is as extremely large as a LOS MIMO system stated in Introduction.

(3) Planar arrays with directional antenna elements will be used for actual MIMO systems. In this paper, we investigate fundamental characteristics in a case where multipath components are very few in radio environments. The simplified assumption of linear arrays with isotropic antenna elements will give a tendency of MIMO systems in such environments.

It is, however, better to investigate the performance under some other antenna parameters. This is future work.

From the assumptions of linear arrays with isotropic antenna elements, we do not need to consider zenith angles, but we treat only azimuth angles on the x-y plane.

3.1 Analog Beam Steering and Precoder Optimization at BS

Here, we describe how the BS works. First, the BS estimates the AODs of multipath components. This is possible using pilot symbols such as a discovery signal [16]. The BS steers the beams of subarrays in multipath directions. In Sect. 5, we will examine in detail how we allocate the beams to multipath components. After adjusting the subarrays, the BS estimates the $M \times N$ channel matrix $\boldsymbol{H}$ from the BS to the UE by sending other pilot symbols. The precoder realizes the optimal transmission by singular value decomposition

of $\boldsymbol{H}$ and power allocation based on water-filling [27].

The power allocation is carried out as stated below. We write the jth eigenvalue of the Gram matrix $\boldsymbol{H}^H \boldsymbol{H}$ as λ_j, where ^{H} denotes the Hermitian transpose, and the total transmit power as P_t. From the water-filling theorem, the optimum power P_j allocated to the jth layer is given by

$$P_j = \max\left(\frac{1}{\alpha} - \frac{P_{\text{noise}}}{\lambda_j}, 0\right), \tag{1}$$

where α is chosen to satisfy the power sum constraint $\sum_j P_j = P_t$, and P_{noise} denotes noise power at the UE. The power ratio to the total power P_t is given by dividing (1) by P_t, and we have

$$p'_j = \frac{P_j}{P_t} = \max\left(\nu - \frac{1}{\frac{P_t}{P_{\text{noise}}}\lambda_j}, 0\right), \tag{2}$$

where $\nu = \frac{1}{\alpha P_t}$. In this paper, we call $\frac{P_t}{P_{\text{noise}}}$ a normalized total transmit power. From (2), we see that when the eigenvalues λ_j are obtained, the BS can allocate optimally the power to each layer for a given normalized total transmit power, and the channel capacity is given by

$$\sum_j \log\left(p'_j \frac{P_t}{P_{\text{noise}}}\lambda_j + 1\right). \tag{3}$$

3.2 Preliminaries to Performance Evaluation of MIMO Systems

In Sect. 5, we evaluate the performance of the hybrid MIMO system in a sub-Terahertz band by simulations. For the evaluations, we analytically obtain several quantities in this subsection.

First, we calculate the (m, n)th element h_{mn} of $\boldsymbol{H}$. We express the nth subarray's pattern as $g_n(\phi; \Phi_n)$, where Φ_n denotes a main beam direction. The pattern is given by

$$g_n(\phi; \Phi_n) = \frac{1}{\sqrt{N_s}}\left\{\frac{\sin\left(\left(\frac{\pi N_s}{2}\right)(\sin\phi - \sin\Phi_n)\right)}{\sin\left(\left(\frac{\pi}{2}\right)(\sin\phi - \sin\Phi_n)\right)}\right\}. \tag{4}$$

According to the channel model proposed in [18], [31], each multipath component arrives at the UE via a time cluster, and the multipath component is also called subpath. We represent the complex amplitude received at the mth antenna from the nth subarray via the kth subpath within the lth time cluster as $r_{m,n,l,k}$. At Step 1 in channel modeling in [31], a TX-RX separation distance is generated. At Step 2 in [31], total received omnidirectional power is determined considering the path loss. The value is the received power when omnidirectional antennas are used at both the TX and RX sides. In this paper, we skip these two steps. This means that when transmit power from an omnidirectional antenna is 1, received power from all the subpaths at an omnidirectional antenna is 1. Skipping the two steps does not affect the fundamental evaluation of MIMO spatial multiplexing. When we deal with actual environments, we have path loss related to the TX-RX separation distance. In such a case,

we can include the effect into the normalized total transmit power defined previously. The impulse response of the above subpath is expressed as

$$a_{l,k} \exp(j\varphi'_{l,k}) g_n(\phi_{l,k,\text{AOD}}; \Phi_n)$$
$$\exp\left[-j(n-1)N_s\pi \sin \phi_{l,k,\text{AOD}}\right]$$
$$\exp\left[-j(m-1)\pi \sin \phi_{l,k,\text{AOA}}\right] \delta(t - \tau_{l,k}), \quad (5)$$

where $a_{l,k}$, $\varphi'_{l,k}$, $\tau_{l,k}$, $\phi_{l,k,\text{AOD}}$, and $\phi_{l,k,\text{AOA}}$ denote the amplitude, phase, propagation delay, AOD from the BS, and angle of arrival (AOA) to the UE of the kth subpath within the lth time cluster, respectively. Here, we choose the phase reference point of BS at the center of subarray #1, and that of UE at the antenna element #1. Moreover, it should be noted that the subarray spacing is $\lambda N_s/2$.

Applying Fourier transform to (5), $r_{m,n,l,k}$ at frequency f is expressed as

$$r_{m,n,l,k} = a_{l,k} \exp(j\varphi_{l,k}) g_n(\phi_{l,k,\text{AOD}}; \Phi_n)$$
$$\exp\left[-j(n-1)N_s\pi \sin \phi_{l,k,\text{AOD}}\right]$$
$$\exp\left[-j(m-1)\pi \sin \phi_{l,k,\text{AOA}}\right], \quad (6)$$

where $\varphi_{l,k}$ is given by

$$\varphi_{l,k} = \varphi'_{l,k} - 2\pi f \tau_{l,k}. \quad (7)$$

In the remainder of this paper, we set the frequency 140 GHz.

The (m, n)th element h_{mn} is given by the total of $r_{m,n,l,k}$ for all the time clusters and subpaths, and hence we have

$$h_{mn} = \sum_l \sum_k r_{m,n,l,k}. \quad (8)$$

4. Channel Properties at Sub-Terahertz Band

Since channel properties affect the performance of MIMO systems, we examine sub-Terahertz band properties in this section. Reference [18] states that the total number of multipath components at 140 GHz is much fewer than the number at 28 GHz, and that the 140 GHz channel is much sparser than the channel at 28 GHz. The reason for this is due to the higher partition loss at 140 GHz. Here, partition loss is defined as the difference between signal power right before the partition and the signal power right after the partition, which includes reflection/scattering loss and the material absorption loss [32].

The following are more quantitative results stated in [18]. As seen from Fig. 4 in [18], in almost all LOS cases, the number of time clusters of 140 GHz is equal to or less than 3. Figure 5 shows that in about 80 percent cases, the number of subpaths within a cluster is one or two. Thus, it is conjectured that in most LOS scenarios, the total number of subpaths or multipath components in a sub-Terahertz band is equal to or less than six. This is consistent with the results in Table VII in [18].

A time cluster comprises multipath components traveling close in time, and multiple time clusters can arrive at unique pointing angles [31]. The reference [18] states that

Table 1 Simulation parameters.

Number of subarrays at BS (N)	8
Number of antennas per subarray at BS (N_s)	64
Number of antennas at UE (M)	8
Number of trials	1000

Table 2 Channel model parameters.

TC#	SP#	Delay [ns]	Power	Amplitude	Average AOD [deg]	Average AOA [deg]
1	1	0.0	0.2734	0.5228	0	180
	2	0.8	0.1855	0.4308		
2	1	6.8	0.1669	0.4085	35	120
	2	7.0	0.1494	0.3866		
3	1	13.0	0.1532	0.3915	35	120
	2	14.5	0.0715	0.2674		

there are at most two main directions of arrival or departure at 140 GHz in the measurement environment. Thus, if there are three time clusters, at least two of them have the same main directions, i.e. the same average angles. This is the case that we treat in the next section.

5. Simulations

We evaluated the performance of the hybrid MIMO system for a 140 GHz LOS indoor scenario. The simulation parameters are listed in Table 1. Table 2 shows the channel model parameters obtained based on [18]. "TC#" and "SP#" denote the time cluster number and the subpath number, respectively. "Delay" represents the excess time delay for (TC#, SP#) with respect to (TC 1, SP 1). "Power" for (TC#, SP#) was calculated using "Delay." "Amplitude" was given by the square root of "Power," and is $a_{l,k}$ in Sect. 3. The phase $\varphi'_{l,k}$ was given by a uniform random number between 0 and 2π for each trail. The azimuth angle of departure $\phi_{l,k,\text{AOD}}$ was given by a normal random number with "Average AOD" and a standard deviation of 4.3 deg. Similarly, the azimuth angle of arrival $\phi_{l,k,\text{AOA}}$ was given by a normal random number with "Average AOA" and a standard deviation of 4.4 deg. Both the standard deviations are measured values in the environment [18]. We used them also for the simulation. Changing these values, we conducted 1000 trails.

Table 3 lists allocated beams to the sets of time cluster and subpath, (TC#, SP#). For example, as for "Beam allocation D," the beams of subarrays #1 and #2 were steered to (TC#, SP#) = (1, 1), beams of subarrays #3 and #4 were steered to (1, 2). The beams of subarrays #5, #6, #7, and #8 were steered to (2, 1), (2, 2), (3, 1), and (3, 2), respectively. In "Beam allocation D," all the beams were steered to all the multipath components. In the table, N/A stands for "not allocated." This means that no beam is allocated to the corresponding (TC#, SP#). Note that the resolution of allocation was 1 deg. Thus, the main beam direction Φ_n in (4) was an integer nearest to the corresponding AOD, $\phi_{l,k,\text{AOD}}$.
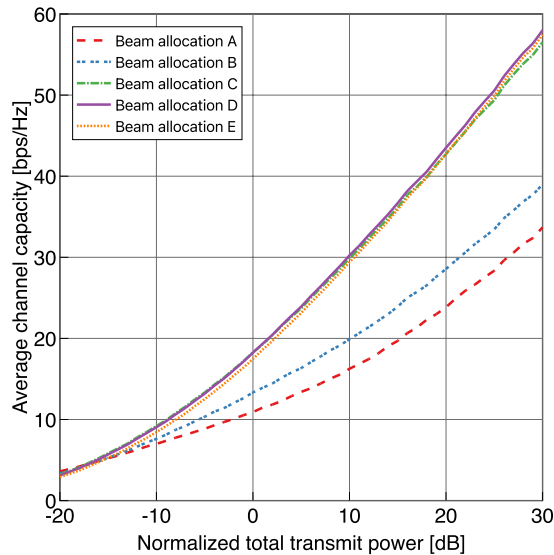
Figure 2 shows the average channel capacity obtained by (3) versus normalized total transmit power for different

**Table 3**   Beam allocation to time cluster and subpath.

(TC#, SP#)	Beam allocation				
	A	B	C	D	E
(1, 1)	1-8	1-4	1, 2	1, 2	1
(1, 2)	N/A	5-8	3, 4	3, 4	2
(2, 1)	N/A	N/A	5, 6	5	3
(2, 2)	N/A	N/A	7, 8	6	4
(3, 1)	N/A	N/A	N/A	7	5, 6
(3, 2)	N/A	N/A	N/A	8	7, 8

The above numbers denote corresponding subarrays

Fig. 2   Average channel capacity versus normalized total transmit power for different beam allocation.

beam allocation. It is clearly seen that the channel capacity for "Beam allocation A and B" are poor compared with the other allocation schemes. All the beams for "Beam allocation A" were steered to (TC#, SP#) = (1, 1), and the beams for "Beam allocation B" were formed toward (1, 1) and (1, 2), which were closely located each other. For the other allocation, the beams were steered to different time clusters, which were largely separated. We see almost the same performance for "Beam allocation C, D, E." Among them, "Beam allocation D" yields slightly higher channel capacity than the others. From these results, it is conjectured that the analog beams should be steered to all the multipath components to achieve higher channel capacity. Specifically, good performance is obtained when we allocate an analog beam to each multipath component and doubly allocate residual beams to multipath components from the largest one. We examine the reason for the difference of channel capacitiy in detail in the following.

Figure 3 plots cumulative distributions of eigenvalues of the Gram matrix $\boldsymbol{H}^H \boldsymbol{H}$ for "Beam allocation A and D." We have only six multipath components as shown in Table 2. Although the channel matrix $\boldsymbol{H}$ is 8×8, the rank is six. Thus, we have only six positive eigenvalues. This is the reason why only six curves are drawn in each figure. It is seen that the first eigenvalues for "Beam allocation D" are lower
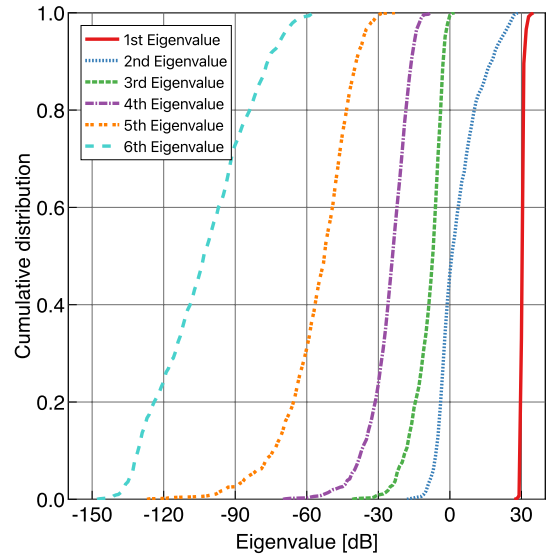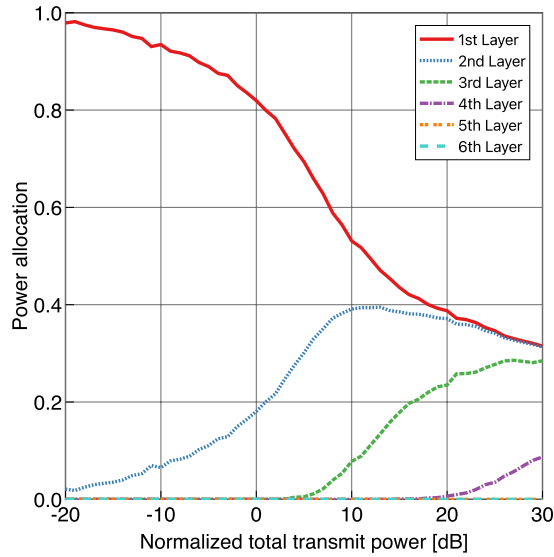

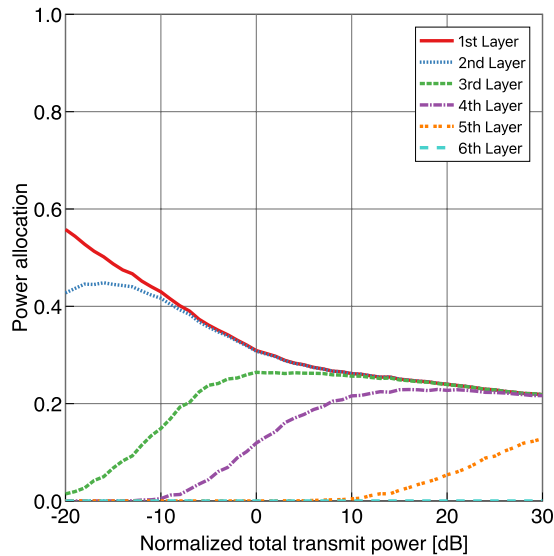(a) Beam allocation A
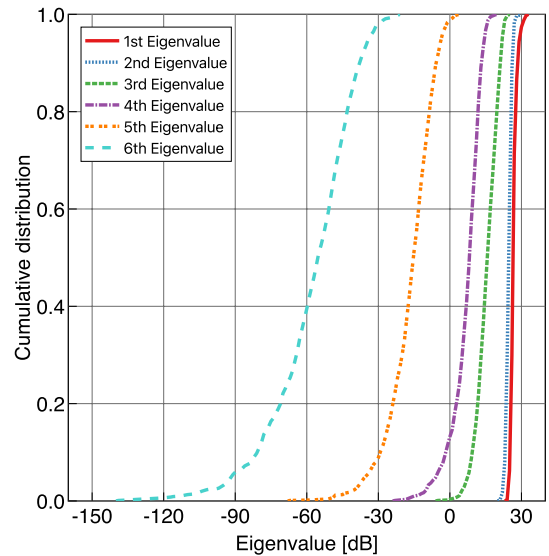
(b) Beam allocation D

Fig. 3   Cumulative distributions of eigenvalues of $\boldsymbol{H}^H \boldsymbol{H}$ for beam allocation A and D.

than those for "Beam allocation A." The other eigenvalues for "Beam allocation D" are, however, larger than those for "Beam allocation A." Thus, although the channel capacity of the first layer for "Beam allocation D" is lower than that for "Beam allocation A," the other channel capacity is higher than that for "Beam allocation A."

Figure 4 shows power allocation given by (2) versus normalized total transmit power for "Beam allocation A and D." The curve for the 5th layer is identical with that for the 6th layer for "Beam allocation A", and is not seen in Fig. 4(a). We see that for any normalized total transmit power, "Beam allocation D" has more allocated layers than "Beam allocation A," and has higher multiplexing gain. This is the reason why "Beam allocation D" has much higher channel capacity than "Beam allocation A."

(a) Beam allocation A

(b) Beam allocation D

Fig. 4 Power allocation versus normalized total transmit power for beam allocation A and D.

Fig. 5 Channel correlation versus beam pair for beam allocation A and D.

Now, we consider correlations between beams, or correlations between subarrays. The normalized non-diagonal (p, q)th component of $\boldsymbol{H}^H\boldsymbol{H}$ is the channel correlation of the beam pair $[p, q]$ for the corresponding channel matrix $\boldsymbol{H}$. Thus, the absolute value of the correlation is given by

$$\frac{\left| \sum_{m=1}^{M} h_{mp}^* h_{mq} \right|}{\sqrt{\sum_{m=1}^{M} |h_{mp}|^2 \sum_{m=1}^{M} |h_{mq}|^2}} \quad \text{for } p \neq q, \tag{9}$$

In the remainder of this paper, we refer to the absolute values of correlations simply as correlations. We averaged the correlations over 1000 sets of channels.
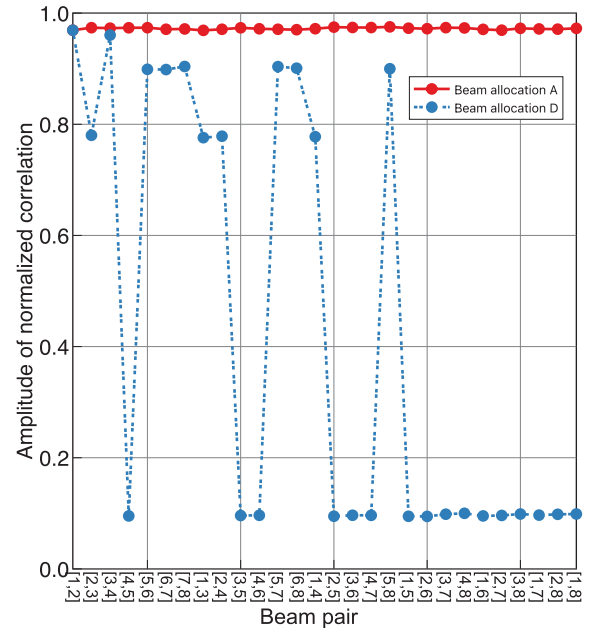
Figure 5 plots the correlations of the beam pairs for "Beam allocation A and D." In the figure, the beam pair $[1, 2]$ is a set of the beams generated by the subarrays #1 and #2, and the other pairs are defined in the same manner. We clearly see that the correlations for "Beam allocation A" are close to 1 for all the beam pairs. This is proved in the following:

All the beams are steered to (TC#, SP#) = (1, 1) for "Beam allocation A," and they greatly reduce all the other multipath components. Thus, using (6) and (8), h_{mn} can be approximated by

$$h_{mn} \simeq a_{1,1} \exp(j\varphi_{1,1}) g_n(\phi_{1,1,\text{AOD}}; \Phi_n)$$
$$\exp\left[-j(n-1)N_s\pi \sin \phi_{1,1,\text{AOD}}\right]$$
$$\exp\left[-j(m-1)\pi \sin \phi_{1,1,\text{AOA}}\right]. \tag{10}$$

Note that $a_{1,1} \exp(j\varphi_{1,1})$ is the complex amplitude of the multipath component from (TC#, SP#) = (1, 1). Furthermore, we have

$$h_{mp}^* h_{mq} \simeq a_{1,1}^2 g_p(\phi_{1,1,\text{AOD}}; \Phi_p) g_q(\phi_{1,1,\text{AOD}}; \Phi_q)$$
$$\exp\left[j(p - 1)N_s\pi \sin \phi_{1,1,\text{AOD}}\right]$$
$$\exp\left[-j(q - 1)N_s\pi \sin \phi_{1,1,\text{AOD}}\right]. \tag{11}$$

$$\left| \sum_{m=1}^{M} h_{mp}^* h_{mq} \right|$$
$$\simeq M a_{1,1}^2 \left| g_p(\phi_{1,1,\text{AOD}}; \Phi_p) g_q(\phi_{1,1,\text{AOD}}; \Phi_q) \right|. \tag{12}$$

Similarly, we have

$$\sum_{m=1}^{M} |h_{mp}|^2 \simeq M a_{1,1}^2 g_p^2(\phi_{1,1,\text{AOD}}; \Phi_p). \tag{13}$$

$$\sum_{m=1}^{M} |h_{mq}|^2 \simeq M a_{1,1}^2 g_q^2(\phi_{1,1,\mathrm{AOD}}; \Phi_q). \tag{14}$$

Thus, we see that the correlation is close to 1 for "Beam allocation A" as below:

$$\frac{\left|\sum_{m=1}^{M} h_{mp}^* h_{mq}\right|}{\sqrt{\sum_{m=1}^{M} |h_{mp}|^2 \sum_{m=1}^{M} |h_{mq}|^2}}$$

$$\simeq \frac{M a_{1,1}^2 \left| g_p(\phi_{1,1,\mathrm{AOD}}; \Phi_p) g_q(\phi_{1,1,\mathrm{AOD}}; \Phi_q) \right|}{M a_{1,1}^2 \left| g_p(\phi_{1,1,\mathrm{AOD}}; \Phi_p) g_q(\phi_{1,1,\mathrm{AOD}}; \Phi_q) \right|}$$

$$= 1. \tag{15}$$

The approximation (10) depends on the subarray architecture. If the main beam is wider and side lobes are higher such as the case of $N_s = 16$, h_{mn} includes higher contributions from multipath components other than (TC#, SP#) = (1, 1). In this case, the correlations for "Beam allocation A" are lower than those in Fig. 5.

On the other hand, the correlations for "Beam allocation D" are significantly different depending on beam pairs. The results for "Beam allocation D" are summarized as follow:

(1) As stated previously, the beams of the subarrays #1 and #2 were steered to (TC#, SP#) = (1, 1), namely in the same direction. Thus, the correlation of the beam pair [1, 2] is close to 1.

(2) The beams of the subarrays #2 and #3 were formed to (1, 1) and (1, 2), respectively, and hence the beam directions were slightly separated. This is the reason why the correlation of the beam pair [2, 3] is fairly lower than 1, about 0.78.

(3) It is seen that the correlation of the beam pair [4, 5] is very low, about 0.1. The beams of subarrays #4 and #5 were steered to (1, 2), and (2, 1), respectively. The multipath components of (1, 2) and (2, 1) belong to the different time clusters, which are located far apart, and the beam directions are largely separated. Thus, the correlation is extremely low. The correlations of the other beam pairs can be explained in the same manner.

The lower correlations for "Beam allocation D" enlarge eigenvalues of $\boldsymbol{H}^H \boldsymbol{H}$ other than the first one, and improve the channel capacity.

We evaluated the performance also for $N_s = 16$, and we confirmed that the basic tendency is the same, although the performance is worse than that for $N_s = 64$. In addition, it is also confirmed that almost the same results for beam allocation were obtained in some other cases with different channel model parameters.

6. Conclusions

Since it has been recently reported that multipath components are very few in a sub-Terahertz band in indoor environments, we have examined spatial multiplexing of a hybrid MIMO system in this band. Through simulation results,

we have revealed that the analog beams should be steered to all the multipath components to lower correlations and to achieve higher channel capacity.

In the simulation, we assumed six multipath components in the environment. We may, however, have many cases where the number of multipath components is less than six [18]. In such pessimistic scenarios, one of the promising schemes is modify environments. The concept is called smart radio environments (SREs) which can be realized using reconfigurable intelligent surfaces (RISs) [33]. To this end, researchers will need wide knowledge ranging from electromagnetic waves to information theory as the authors of [33] say:

"Owing to the interdisciplinary essence of RIS-empowered SREs, finally, we put forth the need of reconciling and reuniting C. E. Shannon's mathematical theory of communication with G. Green's and J. C. Maxwell's mathematical theories of electromagnetism for appropriately modeling, analyzing, optimizing, and deploying future wireless networks empowered by RISs."

Reprinted from [33] with permission (©2020 IEEE).

References

[1] Oulu University, "White paper on 6G networking — 6G Research Visions," no.6, June 2020. ISBN9789526226842

[2] NTT DoCoMo, "White paper: 5G Evolution and 6G," ver. 3, Feb. 2021.

[3] H. Viswanathan and P.E. Mogensen, "Communications in the 6G era," IEEE Access, vol.8, pp.57063–57074, March 2020. DOI: 10.1109/ACCESS.2020.2981745

[4] M. Giordani, M. Polese, M. Mezzavilla, S. Rangan, and M. Zorzi, "Toward 6G networks: Use cases and technologies," IEEE Commun. Mag., vol.58, no,3, pp.55–61, March 2020. DOI: 10.1109/MCOM.001.1900411

[5] W. Jiang, B. Han, M.A. Habibi, and H.D. Schotten, "The road towards 6G: A comprehensive survey," IEEE Open J. Commun. Soc., vol.2, pp.334–366, Feb. 2021. DOI: 10.1109/OJCOMS.2021.3057679

[6] E. Dahlman, G. Mildh, S. Parkvall, P. Persson, G. Wikström, and H. Murai, "5G evolution and beyond," Trans. IEICE Commun., vol.E104-B, no.9, pp. 984–991, Sept. 2021. https://doi.org/10.1587/transcom.2020FGI0001

[7] I.F. Akyildiz, J.M. Jornet, and C. Han, "Terahertz band: Next frontier for wireless communications," Phys. Commun., vol.12, no.2, pp.16–32, Sept. 2014.

[8] K. Sengupta, T. Nagatsuma, and D.M. Mittleman, "Terahertz integrated electronic and hybrid electronic-photonic systems," Nature Electron., vol.1, no.12, pp.622–635, Dec. 2018.

[9] T. Kawanishi, "THz and photonic seamless communications," IEEE/OSA J. Light. Technol., vol.37, no.7, pp.1671–1679, April 2019.

[10] T.S. Rappaport, Y. Xing, O. Kanhere, S. Ju, A. Madanayake, S. Mandal, A. Alkhateeb, and G.C. Trichopoulos, "Wireless communications and applications above 100 GHz: Opportunities and challenges for 6G and beyond," IEEE Access, vol.7, pp.78729–78757, June 2019. DOI: 10.1109/ACCESS.2019.2921522

[11] I.F. Akyildiz and J.M. Jornet, "Realizing ultra-massive MIMO (1024×1024) communication in the (0.06–10) terahertz band," Nano Commun. Netw., vol.8, pp.46–54, June 2016.

[12] C. Han, L. Yan, and J. Yuan, "Hybrid beamforming for terahertz

wireless communications: Challenges, architectures, and open problems," IEEE Wireless Commun. Mag., vol.28, no.4, pp.198–204, Aug. 2021. DOI: 10.1109/MWC.001.2000458

[13] C. Lin and G.Y. Li, "Terahertz communications: An array-of-subarrays solution," IEEE Commun. Mag., vol.54, no.12, pp.124–131, Dec. 2016. DOI: 10.1109/MCOM.2016.1600306CM

[14] F. Sohrabi and W. Yu, "Hybrid digital and analog beamforming design for large-scale antenna arrays," IEEE J. Sel. Top. Signal Process., vol.10, no.3, pp.501–513, April 2016. DOI: 10.1109/JSTSP.2016.2520912

[15] S. Suyama, T. Okuyama, Y. Kishiyama, S. Nagata, and T. Asai, "A study on extreme wideband 6G radio access technologies for achieving 100 Gbps data rate in higher frequency bands," IEICE Trans. Commun., vol.E103-B, no.9, pp.992–999, Sept. 2021. https://doi.org/10.1587/transcom.2020FGI0002

[16] T. Obara, S. Suyama, J. Shen, and Y. Okumura, "Joint processing of analog fixed beamforming and CSI-based precoding for super high bit rate massive MIMO transmission using higher frequency bands," IEICE Trans. Commun., vol.E98-B, no.8, pp.1474–1481, Aug. 2015. https://doi.org/10.1587/transcom.E98.B.1474

[17] S.L.H. Nguyen, J. Järveläinen, A. Karttunen, K. Haneda, and J. Putkonen, "Comparing radio propagation channels between 28 and 140 GHz bands in a shopping mall," 12th European Conference on Antennas and Propagation (EuCAP 2018), April 2018. DOI: 10.1049/cp.2018.0874

[18] S. Ju, Y. Xing, O. Kanhere, and T.S. Rappaport, "Millimeter wave and sub-terahertz spatial statistical channel model for an indoor office building," IEEE J. Sel. Areas Commun., vol.39, no.6, pp.1561–1575, June 2021. DOI: 10.1109/JSAC.2021.3071844

[19] A. Adhikary, E.A. Safadi, M.K. Samimi, R. Wang, G. Caire, T.S. Rappaport, and A.F. Molisch, "Joint spatial division and multiplexing for mm-wave channels," IEEE J. Sel. Areas Commun., vol.32, no.6, pp.1239–1255, June 2014. DOI: 10.1109/JSAC.2014.2328173

[20] L. Zheng and D.N.C. Tse, "Diversity and multiplexing: A fundamental tradeoff in multiple-antenna channels," IEEE Trans. Inf. Theory, vol.49, no.5, pp.1073–1096, May 2003. DOI: 10.1109/TIT.2003.810646

[21] A. Høst-Madsen and A. Nosratinia, "The multiplexing gain of wireless networks," Proc. IEEE Inf. Theory (ISIT), Sept. 2005. DOI: 10.1109/ISIT.2005.1523709

[22] D.W. Yue and H.H. Nguyen, "Multiplexing gain analysis of mmWave massive MIMO systems with distributed antenna subarrays," IEEE Trans. Veh. Technol., vol.68, no.11, pp.11368–11373, Nov. 2019. DOI: 10.1109/TVT.2019.2943663

[23] Special Issue on Adaptive Antennas, IEEE Trans. Antennas Propag., vol.AP-24, no.5, Sept. 1976.

[24] G. Tsoulos, M. Beach, and J. McGeehan, "Wireless personal communications for the 21st century: European technological advances in adaptive antennas," IEEE Commun. Mag., vol.35, no.9, pp.102–109, Sept. 1997. DOI: 10.1109/35.620531

[25] Y. Doi, J. Kitakado, T. Ito, T. Miyata, S. Nakao, T. Ohgane, and Y. Ogawa, "Development and evaluation of the SDMA test bed for PHS in the field," IEICE Trans. Commun., vol.E86-B, no.12, pp.3433–3440, Dec. 2003.

[26] J.H. Winters, "On the capacity of radio communication systems with diversity in a Rayleigh fading environment," IEEE J. Sel. Areas Commun., vol.5, no.5, pp.871–878, June 1987. DOI: 10.1109/JSAC.1987.1146600

[27] E. Telatar, "Capacity of multi-antenna Gaussian channels," Eur. Trans. Telecommn., vol.10, no.6, pp.585–595, Nov./Dec. 1999. DOI: 10.1002/ett.4460100604

[28] Q.H. Spencer, A.L. Swindlehurst, and M. Haardt, "Zero-forcing methods for downlink spatial multiplexing in multiuser MIMO channels," IEEE Trans. Signal Process., vol.52, no.2, pp.461–471, Feb. 2004. DOI: 10.1109/TSP.2003.821107

[29] E. Björnson, L. Perre, S. Buzzi, and E.G. Larsson, "Massive MIMO in sub-6 GHz and mmWave: Physical, practical, and use-case differences," IEEE Wireless Commun. Mag., vol.26, no.2, pp.100–108, April 2019. DOI: 10.1109/MWC.2018.1800140

[30] C.M. Chen, S. Blandino, A. Gaber, C. Desset, A. Bourdoux, L. Perre, and S. Pollin, "Distributed massive MIMO: A diversity combining method for TDD reciprocity calibration," Proc. IEEE Global Commun. Conf. (GLOBECOM), Dec. 2017. DOI: 10.1109/GLOCOM.2017.8254817

[31] M.K. Samimi and T.S. Rappaport, "3-D millimeter-wave statistical channel model for 5G wireless system design," IEEE Trans. Microw. Theory Techn., vol.64, no.7, pp.2207–2225, July 2016. DOI: 10.1109/TMTT.2016.2574851

[32] Y. Xing, O. Kanhere, S. Ju, and T.S. Rappaport, "Indoor wireless channel properties at millimeter wave and sub-terahertz frequencies," Proc. IEEE Global Commun. Conf. (GLOBECOM), Dec. 2019. DOI: 10.1109/GLOBECOM38437.2019.9013236

[33] M.D. Renzo, A. Zappone, M. Debbah, M-S. Alouini, C. Yuen, J. Rosny, and S. Tretyakov, "Smart radio environments empowered by reconfigurable intelligent surfaces: How it works, State of research, and the road ahead," IEEE J. Sel. Areas Commun., vol.38, no.11, pp. 2450–2525, Nov. 2020. DOI: 10.1109/JSAC.2020.3007211

Yasutaka Ogawa received the B.E., M.E., and Ph.D. degrees from Hokkaido University, Sapporo, Japan, in 1973, 1975, and 1978, respectively. Since 1979, he has been with Hokkaido University, where he is currently a Professor Emeritus. During 1992–1993, he was with ElectroScience Laboratory, the Ohio State University, as a Visiting Scholar, on leave from Hokkaido University. His professional expertise encompasses super-resolution estimation techniques, applications of adaptive antennas for mobile communication, multiple-input multiple-output (MIMO) techniques, and measurement techniques. He proposed a basic and important technique for time-domain super-resolution estimation for electromagnetic wave measurement such as antenna gain measurement, scattering/diffraction measurement, and radar imaging. Also, his expertise and commitment to advancing the development of adaptive antennas contributed to the realization of space division multiple accesses (SDMA) in the Personal Handy-phone System (PHS). He received the Yasujiro Niwa Outstanding Paper Award in 1978, the Young Researchers' Award of IEICE in 1982, the Best Paper Award from IEICE in 2007, TELECOM system technology award from the Telecommunications Advancement Foundation of Japan in 2008, the Best Magazine Paper Award from IEICE Communications Society in 2011, the Achievement Award from IEICE in 2014, and the Best Tutorial Paper Award from IEICE Communications Society in 2018. He also received the Hokkaido University Commendation for excellent teaching in 2012. He is a Life Fellow of the IEEE.

Taichi Utsuno received his B.E. degree in electronics and information engineering from Hokkaido University, Sapporo, Japan, in 2020. He is currently a master course student at the Graduate School of Information Science and Technology, Hokkaido University. His research interests are phased arrays and MIMO systems in a sub-Terahertz band.

Toshihiko Nishimura received the B.S. and M.S. degrees in physics and Ph.D. degree in electronics engineering from Hokkaido University, Sapporo, Japan, in 1992, 1994, and 1997, respectively. Since 1998, he has been with Hokkaido University, where he is currently a Professor. His current research interests are in MIMO systems using smart antenna techniques. He received the Young Researchers' Award of IEICE in 2000, the Best Paper Award from IEICE in 2007, and TELECOM System Technology Award from the Telecommunications Advancement Foundation of Japan in 2008, the best magazine paper award from IEICE Communications Society in 2011, and the Best Tutorial Paper Award from the IEICE Communications Society in 2018. He is a member of the IEEE.

Takeo Ohgane received the B.E., M.E., and Ph.D. degrees in electronics engineering from Hokkaido University, Sapporo, Japan, in 1984, 1986, and 1994, respectively. From 1986 to 1992, he was with Communications Research Laboratory, Ministry of Posts and Telecommunications. From 1992 to 1995, he was on assignment at ATR Optical and Radio Communications Research Laboratory. Since 1995, he has been with Hokkaido University, where he is currently a Professor. During 2005–2006, he was at Centre for Communications Research, University of Bristol, U.K., as a Visiting Fellow. His research interests are in MIMO signal processing for wireless communications. He received the IEEE AP-S Tokyo Chapter Young Engineer Award in 1993, the Young Researchers' Award of IEICE in 1990, the Best Paper Award from IEICE in 2007, TELECOM System Technology Award from the Telecommunications Advancement Foundation of Japan in 2008, the Best Magazine Paper Award from IEICE Communications Society in 2011, and the Best Tutorial Paper Award from IEICE Communications Society in 2018. He is a member of the IEEE.

Takanori Sato was born in Hokkaido, Japan, in 1992. He received his Ph.D. degree in the field of media and network technologies from Hokkaido University, Japan, in 2018. He was a Research Fellow of Japan Society for the Promotion of Science (JSPS) from 2017 to 2019. In 2019, he moved to University of Hyogo as an assistant professor. He is currently an associate professor in Hokkaido University. His research interests include the theoretical and numerical studies of optical fibers and photonic circuits using the coupled mode theory and the finite element method. He is a member of the Japan Society of Applied Physics (JSAP), Institute of Electrical and Electronics Engineers (IEEE), and the Optical Society of America (OSA).